Published in final edited form as:
Magn Reson Med. 2012 December ; 68(6): 1774–1784. doi:10.1002/mrm.24186.

Clinically-Compatible MRI Strategies for Discriminating Bound and Pore Water in Cortical Bone

R. Adam Horch[1,2], **Daniel F. Gochberg**[2,3], **Jeffry S. Nyman**[4,5], and **Mark D. Does**[1,2,3,6]

[1]Dept. of Biomedical Engineering, Vanderbilt University

[2]Institute of Imaging Science, Vanderbilt University

[3]Radiology and Radiological Sciences, Vanderbilt University

[4]Department of Veterans Affairs Tennessee Valley Healthcare System, Vanderbilt University

[5]Department of Orthopaedics & Rehabilitation, Vanderbilt University

[6]Electrical Engineering, Vanderbilt University

Abstract

Advances in modern MRI pulse sequences have enabled clinically-practical cortical bone imaging. Human cortical bone is known to contain a distribution of T_1 and T_2 components attributed to bound and pore water, although clinical imaging approaches have yet to discriminate bound from pore water on the basis of their relaxation properties. Herein, two clinically-compatible MRI strategies are proposed for selectively imaging either bound or pore water by utilizing differences in their T_1s and T_2s. The strategies are validated in a population of *ex vivo* human cortical bones, and estimates obtained for bound and pore water are compared to bone mechanical properties. Results show that the two MRI strategies provide good estimates of bound and pore water that correlate to bone mechanical properties. As such, the strategies for bound and pore water-discrimination shown herein should provide diagnostically useful tools for assessing bone fracture risk, once applied to clinical MRI.

Keywords

MRI; bone; bound water; pore water; uTE; T_2

INTRODUCTION

The development of ultrashort-echo time (uTE) and related MRI methods for imaging short T_2 signals (1–5) has generated considerable interest in applying MRI to dense tissues. For example, cortical bone, which is conventionally imaged using X-ray-based methods, can now be effectively imaged with MRI (3,5–9) and its ^{1}H NMR signal characteristics report on bone damage (10) and mechanical properties (11,12). In particular, recent studies show that cortical bone NMR signals of transverse relaxation time constant (T_2) ≈ 400 μs are due primarily to collagen-bound water (13–17) and correlate directly (and more strongly than X-ray based measures) with several mechanical properties of cortical bone (18). Similarly strong inverse correlations were found between signals with T_2 > 1 ms, due primarily to pore water and lipids, and the same mechanical properties (18). These findings demonstrate the potential for MRI to offer diagnostic measures of bone fracture risk, but the opposing

Correspondence to: Mark D. Does, Ph.D., 1161 21st Ave South, AA-1105 MCN, Nashville, TN 37232-2310, mark.does@vanderbilt.edu.

relationships of bound and pore water content with mechanical properties requires MRI methods that distinguish signals from these two biophysical origins. One approach for distinguishing long- from short-T_2 signals in uTE imaging is through T_2 selective RF pulses (19–23). For cortical bone, the broad line widths of both bound and pore water signals (13) dictate the use of relatively high bandwidth RF pulses, which can be realized with intrinsically T_2-selective adiabatic pulses (24,25). Presented here are clinically-practical imaging strategies for distinguishing bound and pore water signals from cortical bone based on T_2-selective adiabatic pulses as well as T_1 characteristics of cortical bone bound and pore water. Signals from each strategy are found to correlate well with previously employed non-imaging methods and with measured bone mechanical properties, demonstrating proof of concept. By way of their compatibility with clinical uTE MRI, the two strategies offer promise for *in vivo* imaging as diagnostic measures of bone fracture risk.

THEORY

A Model for the NMR Lineshape of Water in Cortical Bone

In order to explain the widely different T_2s but apparently similar T_2*s arising from bound and pore water, consider a simple, qualitative model of the observed free induction decay (FID) rate as a sum of reversible and irreversible transverse relaxation rates. That is $R_2^*=R_2+R_2^{'}$, where $R_2^*=1/T_2^*$ is the observed transverse relaxation rate in the FID, $R_2 = 1/T_2$ is the time-irreversible rate as observed in a Carr-Purcell-Meiboom-Gill (CPMG) measurement, and $R_2^{'}$ is the time-reversible rate. With this model, consider bound water to exhibit $R_2 \gg R_2^{'}$ (such that $R_2^* \cong R_2$), a condition of so-called homogenous line-broadening. This arises from dipolar interactions of motionally-restricted bound water spins throughout the bone matrix space, as well as from magnetization transfer with dipolar broadened collagen/semisolids observed in (9,13). Conversely, consider the pore water signal to result from the sum of numerous isolated free water pools, each with relatively low R_2 values but collectively with off-resonant frequencies described by a broad distribution. Such would be the case for the polydisperse pore size distribution observed in bone (e.g. Haversian canals, lacunae, and cannaliculi (15,26)), wherein pores contain motionally-averaged mobile water surrounded by a bone matrix of different magnetic susceptibility (27) that perturbs the local Larmor frequency. Thus, the pore water FID is primarily governed by $R_2^{'}$ (such that $R_2^* \cong R_2^{'}$), a condition of so-called inhomogenous line-broadening. In this sense, cortical bone pore water bears similarity to water within porous media (14). Figure 1 demonstrates NMR frequency-domain representations of this bound/pore water model, and indicates that to effectively manipulate the bulk pore water magnetization a broadband RF pulse is needed to nutate the full distribution of individual off-resonant pore magnetizations within the bulk pore water lineshape.

T_2 Selective Adiabatic RF pulses

From the model above and previous wideline NMR studies (13,28), it is readily apparent that any RF pulse designed to perturb the entire pore water magnetization must possess a relatively large bandwidth (≈ 3500 Hz at 4.7T, estimated ≈ 2000 Hz at 3.0T). A conventional amplitude modulated RF pulse with this bandwidth would be short in duration and similarly responsive for T_2s of both bound and pore water. However, an adiabatic pulse has an additional degree of freedom in design by way of its frequency modulation and can invert spins across a wide bandwidth using a relatively long, frequency-swept RF waveform. Although relaxation during an adiabatic pulse is complicated due to the spectral density contribution at $\gamma B_1(t)$ (29), we approximate such relaxation with the Bloch equations and invariant T_1 and T_2 relaxation time constants. Figure 2 shows the effect of a 5 ms duration, 5 kHz bandwidth hyperbolic secant (sech) adiabatic full passage (AFP) pulse (24) applied to

equilibrium magnetization, as determined by numerical solution of the Bloch equations. This figure demonstrates the T_2-selectivity of such RF pulses, in accord with previous work (22,25), and their suitability for differentially rotating bound water ($T_2 < 1$ ms) and pore water ($T_2 > 1$ ms) magnetizations. The inversion efficiency of a given RF pulse is described by a scalar multiplier ($-1 \leq \alpha \leq 1$) representing the change in longitudinal magnetization caused by each AFP pulse.

Pulse Sequences

Ultra-short echo time—Figure 3a shows a conventional uTE sequence (CuTE), wherein the first data are collected at an ultra-short echo time, typically < 100 μs (1). With such a short echo time, the CuTE signal contains contributions from both bound and pore water, as demonstrated for quantitative bone imaging of total bone water content (7). Acquisition strategies such as a multiple gradient echo or spectroscopic readout (5,30) can be added to CuTE to measure FID signal characteristics for the purpose of discriminating bound from pore water in the T_2* domain. To this end, a spectroscopic method with bi-exponential-T_2* analysis of the uTE signal (herein, BEuTE) has recently been reported (31). In this approach, with a two-compartment model of bound water (bw) and pore water (pw) assuming no inter-compartmental magnetization exchange, the signal magnitude equation for the BEuTE signal is simply,

$$S_{uTE}(TE_i) = S_0^{bw} \sin\theta \frac{1 - e^{-R_1^{bw} TR}}{1 - e^{-R_1^{bw} TR} \cos\theta} e^{-R_2^{*bw} TE_i} + S_0^{pw} \sin\theta \frac{1 - e^{-R_1^{pw} TR}}{1 - e^{-R_1^{pw} TR} \cos\theta} e^{-R_2^{*pw} TE_i}, \quad [1]$$

where TE_i is the time after excitation of the i^{th} signal datum, TR is the sequence repetition time, θ is the excitation pulse flip angle, R_1^{bw} and S_0^{bw} are the longitudinal relaxation rate and relative proton density, respectively, of bound water, and likewise for R_1^{pw} and S_0^{pw} of pore water. Given *a priori* estimates of R_1^{bw} and R_1^{pw}, the observed signal, $S_{uTE}(TE_i)$, can be fitted with Eq [1] to estimate $S_0^{bw,pw}$ and $R_2^{*bw,pw}$. (More on required *a priori* information for this and other sequences below.)

Challenges to the BEuTE approach include potentially similar short T_2* characteristics of bound and pore water (Fig 1) that will likely converge with increasing field strength, off-resonance effects leading to non-monotonic decays, potentially non-lorentzian lineshapes associated with short T_2s, and the need for spectroscopic imaging with sufficient sampling of the ≈ 50 μs to 5 ms TE domain. While practical spectroscopic imaging with bi-exponential fitting has recently been demonstrated in the context of bone MRI (30,31), it has yet to be rigorously evaluated with regards to bound/pore water T_2* discrimination. However, with spectroscopic or multiple gradient echo techniques, bound and pore water should be clearly distinguishable from ∗ surrounding soft tissue signals (marrow, muscle, fat, etc.), which have significantly longer T_2 values (≫ 10 ms) than cortical bone water.

Double Adiabatic Full Passage (DAFP)—A pair of sequential AFP pulses incorporated into the CuTE sequence (Fig 3b) will rotate long-T_2 pore water magnetization through 360° while approximately saturating the bound water magnetization (see Fig 2). Thus, the DAFP signal is comprised primarily of pore water with a magnitude described by

$$S_{DAFP} \approx S_0^{pw} \sin\theta \frac{1 - (\alpha^{pw})^2 e^{-R_1^{pw} TR}}{1 - (\alpha^{pw})^2 e^{-R_1^{pw} TR} \cos\theta} e^{-R_2^{*pw} TE}. \quad [2]$$

Given *a priori* estimates of R_1^{pw} and R_2^{*pw} and knowledge of the inversion efficiency of the AFP pulse on the pore water magnetization, α^{pw}, the pore water proton density, S_0^{pw}, can be estimated from the observed signal, surrounding tissue S_{DAFP}. As noted above, the long-T2 signal may still be suppressed if a multiple gradient echo/spectroscopic readout is employed.

Adiabatic Inversion Recovery (AIR)—An AFP pulse added to the CuTE sequence (Fig 3c) will largely invert pore water while approximately saturating the bound water, following which an appropriate inversion recovery delay (*TI*) can be chosen to null pore water magnetization. Thus, the signal is comprised primarily of bound water with a magnitude described by

$$S_{AIR} \approx S_0^{bw} \sin\theta \frac{1-\left(1-\alpha^{bw}\right)e^{-R_1^{bw}TI}-\alpha^{bw}e^{-R_1^{bw}TR}}{1-\alpha^{bw}e^{-R_1^{bw}TR}\cos\theta} e^{-R_2^{*bw}TE}. \quad [3]$$

If *TI* is chosen to null signal from pore water, this equation can be re-written as

$$S_{AIR} = S_0^{bw} \sin\theta \frac{1-\left(1-\alpha^{bw}\right)\left(\frac{1-\alpha^{pw}e^{-R_1^{pw}TR}}{1-\alpha^{pw}}\right)^{R_1^{bw}/R_1^{pw}}-\alpha^{bw}e^{-R_1^{bw}TR}}{1-\alpha^{bw}e^{-R_1^{bw}TR}\cos\theta} e^{-R_2^{*bw}TE}. \quad [4]$$

Given *a priori* estimates of R_1^{bw}, R_1^{pw}, R_2^{*bw} and α^{bw}, the bound water density, S_0^{bw}, can be estimated from the observed signal, S_{AIR}. Because pore water *R1* is relatively similar to that of surrounding soft tissue (compared with bound water), the AIR sequence will naturally suppress surrounding tissue and has been previously used for this purpose expressly (8,32). But again, as above, this suppression may be further improved through a multiple gradient echo/spectroscopic acquisition.

Absolute Water Concentration—For all of the above measurements, the estimated relative water density, S_0^{bw} or S_0^{pw}, requires an *a priori* estimate of one or more of R_1, R_2^*, or a, for bound and/or pore water, as indicated in Eqs [1–4]. Previous work indicates that across individuals mean R_2^{bw} is relatively constant (13). One can expect R_2^{*bw}, R_1^{bw} and α^{bw} to be so as well, making the choice of their values relatively unimportant as long as the same value is used for calculating S_0^{bw} across individuals. Pore water signal characteristics are more likely to vary across individuals with different pore sizes, so some variation in R_1^{pw}, R_2^{*pw}, and α^{pw} is expected (due to the pore geometry dependence of R_2^{pw} (15,16)). In practice, using a reasonably short echo time (TE < 100 μs) mitigates the importance of the *a priori* estimate of R_2^{*pw}, and the impact of variations in R_1^{pw} and α^{pw} across a small (N = 14) collection of bone samples is evaluated below.

MATERIALS AND METHODS

The proposed pulse sequences and signal equations were evaluated with the following procedure:

1. Establish population-averages of the required *a priori* parameter estimates ($R_1^{bw,pw}$ and $\alpha^{bw,\,pw}$).

2. Measure the relative contributions of bound and pore water to BEuTE, CuTE, DAFP and AIR methods by bi-exponential T_2* (BEuTE) or multi-exponential T_2 characterization (CuTE/DAFP/AIR) of their signals.
3. Correlate estimates of S_0 from BEuTE, CuTE, DAFP and AIR signals to reference-standard equilibrium CPMG measurements and to cortical bone mechanical properties.

Human cortical bone preparation

The Musculoskeletal Tissue Foundation (Edison, NJ), a non-profit tissue allograft bank, and the Vanderbilt Donor Program (Nashville, TN) supplied human femurs from 14 cadaveric donors (8 male, 6 female, 22–98 years old, mean ± standard deviation (SD) = 70 ± 25 years) under instruction to not provide tissue from donors who had tested positive for a blood borne pathogens. Cortical bone specimens for either NMR or mechanical testing were extracted under irrigation from adjacent sites in the medial mid-shaft of each donor's right femur and were machined to ≈ 10×2×4 mm or 40×2×4 mm dimensions, respectively, providing uniform cortical bone, free of endosteal and periosteal surfaces. Note that volume of the NMR samples, determined by digital caliper measurement, was on the order one or a few voxels in a typical lower leg quantitative uTE bone image (6). Specimens were stored in phosphate-buffered saline at −80 °C between processing and measurements, and specimens were thawed at 4 °C approximately 18 hours prior to measurements. Immediately prior to NMR measurements, thawed specimens were removed from PBS and blotted dry to remove pooled surface water.

Mechanical Testing

Standard three-point bend mechanical testing was performed at room temperature to determine several mechanical properties relevant to fracture risk in bone: flexural modulus, yield stress, peak stress, fracture stress, and toughness to failure. A material testing system (Dynamight 8841; Instron, Canton, OH) recorded the force-displacement data from a 100 Newton load cell and the linear variable differential transformer at 50 Hz. Hydrated bone was loaded to failure at 5 mm/min on a 35 mm support span. Various mechanical properties were determined from force-displacement data following the standard methods described previously (18).

NMR

NMR measurements were performed at 200 MHz and ≈ 20°C using a 4.7T horizontal bore magnet with a DirectDrive console (Varian/Agilent, Santa Clara, CA). An in-house loop-gap style RF coil with Teflon structural support was used (similar to the coil described in (33)), which provided 90°/180° RF pulses of ≈ 5 μs/10 μs duration and contributed negligible background ^{1}H signal (<1% of net cortical bone signal). In all NMR measurements, bone specimens were placed with osteonal direction orthogonal to B_0 to maintain consistent magic angle effects. In all measurements of the CuTE, DAFP, and AIR sequences, a microsphere containing 21.2 μL of deionized H_2O (T_2 ≈ 2.5 s) was placed adjacent to bone specimens as a reference marker for signal size quantitation. Also, to ensure there were no significant time-dependent changes of the bone T_2 characteristics during NMR measurements, equilibrium CPMG measurements were collected before and after each series of measurements.

Using experimental parameters described elsewhere (13), transverse relaxation was measured at equilibrium with a CPMG pulse sequence (100 μs echo spacing), and longitudinal relaxation was characterized with inversion-recovery-prepared CPMG (IR-CPMG). To observe the effects of a single AFP pulse on bound and pore water signals in

cortical bone (α^{bw} and α^{pw}), the CPMG measurements were repeated with and without a preparatory sech pulse (AFP-CPMG) of varying duration and bandwidth (combinations of 5,10,15 ms and 1,2,3.5,5 kHz were utilized). During a 5 ms delay between the sech pulse and the excitation RF of the CPMG acquisition, a spoiler gradient (2 ms, 10 G/cm) removed any net transverse magnetization.

CuTE and DAFP and AIR sequences were driven to steady state by replacing their uTE imaging modules (Fig 3) with a non-imaging acquisition: hard RF excitation (10 μs, 20°) followed by an FID acquisition and a subsequent spoiler gradient (5 ms, 10 G/cm). FID and CPMG acquisitions were collected at steady state. The DAFP and AIR sequences used sech pulses of 10 ms duration and 3.5 kHz BW. (These pulses used ≈ 24 μT peak B_1, which is near the maximum available on typical human MRI systems but can be reduced by using higher order hyperbolic secant, HSn, pulses (34)). Both AIR and DAFP used TR = 300 ms; CuTE used TR = 35 ms. AIR measurements were repeated with 11 TI values spanning 70–110 ms to empirically determine a single optimal TI for nulling pore water across all specimens (minimal signal in T_2 spectral pore water domain).

The BEuTE method was evaluated by analyzing non-imaging FIDs collected from equilibrium magnetization (pulse-acquire measurement: TR = 5 s, 90° flip, acquisition of a 10 ms window at 2.5 MHz bandwidth, 64 averages, 8 μs receiver dead time prior to acquisition). These equilibrium FIDs provide an idealized test bed for evaluating the BEuTE method, as they are free of imaging artifacts and unwanted coherence pathways potentially present in the steady state imaging version of BEuTE. Bound and pore water T_1-weighting, which is not present in the equilibrium FIDs but would be in BEuTE imaging, is not required to evaluate the soundness of the BEuTE method.

Data Analysis

All data processing was performed using MATLAB (The Mathworks, Natick, MA). The freely-available MERA_Toolbox (Multi-Exponential Relaxation Analysis, http://vuiis.vanderbilt.edu/~doesmd/MERA/MERA_Toolbox.html) provided a regularized non-negative least-square (NNLS) approach to estimate multi-exponential T_2 spectra from CPMG data and T_1-T_2 spectra from IR-CPMG data as described in (13). Because AFP-CPMG measurements contained decaying signals of both positive and negative amplitude, direct NNLS analysis was not possible. Instead, the complex AFP-CPMG signals were first summed with the complex equilibrium-CPMG signals, and the resulting summed signal, comprised solely of non-negative amplitude decaying exponentials, was fitted with a T_2 spectrum. This T_2 spectrum was then subtracted on a peak-by-peak basis from the equilibrium T_2 spectrum to construct an estimated AFP-CPMG T_2 spectrum.

Population averaged bound/pore R_1s were computed from each specimen's T_1-T_2 spectra by computing the mean R_1 in the appropriate T_2 domains (for bound and pore water) and the resulting R_1s were averaged across all specimens. A population average for net water R_1 (R_1^{nw}) was similarly computed from mean R_1s across both bound and pore water T_2 domains. Population averaged AFP efficiency parameters, α^{bw} and α^{pw} were estimated by dividing bound or pore water T_2 spectral intensities from the AFP-CPMG measurements by those from the equilibrium CPMG measurements and then averaging across specimens.

Steady state longitudinal magnetizations of CuTE, DAFP, and AIR pulse sequences were discriminated on a T_2 basis via NNLS fitting of CPMG data collected in the final TR periods. CuTE CPMG data satisfied the NNLS constraint, so fitting directly gave T_2 spectra. However DAFP and AIR CPMGs potentially contained both positive and negative decays, so T_2 spectra were calculated in the same manner as those from AFP-CPMG data (described above).

FIDs from the CuTE, DAFP, and AIR sequences were quantified similarly to previous in vivo studies that employ reference signals (6,7), although transverse relaxation decay during TE periods was not considered (assumed TE $\ll T_2$* in all sequences). FID magnitudes at TE = 50 μs, which consisted of both short-T_2* bone water and long-T_2* marker water, were stripped of long-T_2* marker water contributions by subtracting magnitudes at TE = 3 ms, and the resulting signal was defined as S_{CuTE}, S_{DAFP}, or S_{AIR}. (When imaging, the reference signal would be spatially resolved from cortical bone and so the long-TE signal subtraction would only be used to suppress contaminating soft tissue signals.) S_{CuTE} and R_1^{nw} were then used with a mono-exponential form of Eq [1] (i.e. the standard spoiled gradient echo signal equation) to estimate the net water proton density, S_0^{nw}, while S_{DAFP}, S_{AIR} and the appropriate population-averaged *a priori* parameter estimates were used with Eq [2] or [3] to estimate S_0^{bw} or S_0^{pw}. To convert S_0^{nw}, S_0^{bw}, and S_0^{pw} into units of absolute proton concentration, these estimates were multiplied by $V_{\mathrm{ref}}\rho_{\mathrm{ref}}/V_{\mathrm{bone}}S_0^{\mathrm{ref}}$, where V_{ref} and V_{bone} are the water reference and bone volumes, respectively, ρ_{H_2O} = 111.1 mol ^{1}H/L$_{H_2O}$ was the assumed proton concentration of the reference, and S_0^{ref} is the total signal arising from the water marker (obtained by integrating the equilibrium CPMG T_2 spectrum over T_2s > 1000 ms, where the entire marker signal is clearly discriminated from bone water). Resulting proton concentration estimates from the CuTE, DAFP, and AIR signals were pairwise linearly regressed to the aforementioned bone mechanical properties, as well as to reference-standard measures of net, pore, and bound water, respectively. These reference-standard measures were calculated from equilibrium CPMG-derived T_2 spectra by integrating over the appropriate T_2 domains, as previously demonstrated in (13,18).

Equilibrium FIDs, chosen as surrogates to BEuTE signals (see rationale above), were fit with bi-exponential decays via least-squares fitting to Eq [1], assuming $e^{-R_1 TR} \approx 0$ (i.e. TR $\gg T_1$). FIDs were fit across a time domain of 50 μs to 4.5 ms (similar to that shown in the aforementioned bone bi-exponential imaging study (31)) to isolate bound and pore water decays while avoiding signal from a large matrix-related $T_2 \approx 10$ μs component. Resulting short and long-T_2* signal fractions were compared to the fractions of bound and pore water (relative to total water) determined from reference-standard equilibrium CPMG T_2 spectra. While this gave a straightforward evaluation of BEuTE's ability to discriminate bound and pore water, short and long-T_2* signal sizes were also converted to units of proton concentration (via the aforementioned $V_{\mathrm{ref}}\rho_{\mathrm{ref}}/V_{\mathrm{bone}}S_0^{\mathrm{ref}}$ factor), which were pairwise linearly regressed to bone mechanical properties for the purpose of comparing the diagnostic utility of BEuTE to that of CuTE, DAFP, and AIR. Since the water reference was not present during equilibrium FID measurements (to avoid confounding off-resonance effects), this quantitation step used water reference signals acquired in separate experiments, which introduced another source of experimental variance but was expected to be negligible (on the order of 5% of the water reference's signal size (13)).

RESULTS

For the equilibrium CPMG measurements, mean ± SD signal-to-noise ratio (SNR) was 9500 ± 4500, ranging 4200–21000. At the lowest CPMG SNR, Monte Carlo simulation (not shown) indicated that the uncertainties (SD as a percentage of mean) in CPMG-derived T_2 spectral pool sizes were ≈ 3% for bound and pore water; at typical SNR of 9500, uncertainties dropped to ≈ 1.0%. Figure 4A shows representative cortical bone T_2 spectra collected with and without a 5 ms duration, 5 kHz bandwidth AFP preparatory pulse. It is clear that the AFP pulse largely saturates the submillisecond-T_2 bound water while strongly inverting the long-lived pore water T_2s. These effects are shown in Fig 4B on a peak-wise basis for three specimens subjected to various AFP bandwidths; similar results (not shown)

were obtained at the other AFP pulse durations. All but the narrowest bandwidth AFP pulses generally trended with the simulations (e.g. Fig 2), although some positive bias is generally observed. The narrowest bandwidth AFPs (1000 Hz) all failed to strongly invert long-T_2 pore water. The α^{bw} was extracted from the 10ms/3.5kHz AFP-CPMG data and ranged 0.08–0.11 (mean ± SD: 0.09 ± 0.01) across all specimens, while α^{pw} ranged from −0.90 to −0.65 (mean ± SD: −0.78 ± 0.07). These mean α^{bw} and α^{pw} values were used in all signal quantitation.

T_1-T_2 spectra from IR-CPMG resembled those shown elsewhere (13). As previously described, population-averaged pool T_1s extracted from these spectra were used in all signal quantitation. Bound water T_1s were consistent across specimens, ranging 340–370 ms (mean ± SD: 357 ± 10 ms), while pore water T_1s exhibited a wider range of 380–775 ms (mean ± SD: 551 ± 120). Net T_1s (weighted average of bound and pore water) ranged 380–450 ms (mean ± SD: 412 ± 20 ms).

Bi-exponential fitting results for evaluating the BEuTE method are given in Fig 5. Across the specimens, the short-T_2* component ranged 230–370 μs (mean ± SD: 290 ± 40), while the long-T_2* component ranged 520–1800 μs (mean ± SD: 1280 ± 360). A representative fit is shown in Fig 5A. The signal fractions of the long-T_2* component ranged 0.01–0.25 across specimens (mean ± SD: 0.10 ± 0.06) and were in poor agreement with the long-T_2 signal fractions derived from equilibrium CPMG measurements (Fig 5B), which ranged 0.14–0.61 (mean ± SD: 0.29 ± 0.10). The large bias and lack of trending in Fig 5B shows that signal fractions obtained from the BEuTE method are poor indicators of CPMG signal fractions, the latter of which are known to represent bound/pore water content (13–17).

T_2-resolved signal components present in the CuTE, DAFP, and AIR signals are shown in Fig 6A–C. Bound, pore, or net water proton concentrations determined from each strategy are compared to reference-standard equilibrium-CPMG-derived concentrations in Fig 6D–F, and there was a strong linear correlation ($r^2 \geq 0.7$, $p < 0.05$) in all cases. CuTE/DAFP/AIR-derived proton concentrations agreed well with with net/pore/bound water concentrations derived from equilibrium CPMG, with no statistically significant bias (dashed lines in Fig 6D–F are 95% confidence intervals, which included the line of unity in all cases). For the AIR sequence, a single *TI* of 90 ms was found to give the best pore water suppression across all specimens.

Figure 7 shows correlations between mechanical properties and water concentrations derived from BEuTE/CuTE/AIR/DAFP signals, which are closely analogous to the clinical imaging pixel intensities that could be obtained from these methods. An example of correlations to peak stress is given in Fig. 7A, and Pearson's r^2 between the different strategies and mechanical parameter pairings are given in Fig 7B. BEuTE and CuTE failed to give any statistically significant correlation ($p > 0.05$ in all cases), but AIR and DAFP correlated well to all mechanical properties (r^2 ranged 0.35 to 0.69, $p < 0.05$).

DISCUSSION

Discrete transverse relaxation components of the ^{1}H NMR signal have been well characterized in cortical bone (13–17,28). Relevant to this study, a dominant T_2 component of ≈ 400 μs and a broad distribution of components spanning 1ms - 1 s have been consistently observed in numerous human cadaveric donors. Through a variety of techniques such as H_2O/D_2O exchange, the 400 μs T_2 signal has been attributed to matrix-bound water and the longer-lived signals to pore space water (12,13,35). Recently, a direct linear correlation between the bound water signal size and important mechanical properties such as peak stress has been observed, indicating that, in principle, MRI signals can be used to

assess bone fracture risk (18). However, an inverse linear correlation with the pore water signal size results in a complete loss of predictive power if both bound and pore water contributions are included in the same MRI measurement. Thus, diagnostically-relevant cortical bone image contrast relies on discriminating bound from pore water. To this end, we present a qualitative model of cortical bone relaxation, wherein the bound and pore water signals undergo predominantly homogenous and inhomogenous line-broadening (i.e. irreversible and reversible transverse relaxation), respectively. In light of this model, we evaluate clinically-applicable uTE-compatible AIR and DAFP schemes for quantitative bound and pore water signal discrimination, which would act as surrogates to the diagnostically-useful but clinically-impractical CPMG measurements in (13,18). Undiscriminated water signal quantitation has been successfully implemented on clinical scanners (6,7) via phantoms with known composition and NMR parameters, and we demonstrate an analogous procedure herein with the AIR and DAFP strategies to demonstrate their bound or pore water selectivity in comparison to existing BEuTE/CuTE bone imaging methods.

A Model for Cortical Bone Bound and Pore Water Transverse Relaxation

The model of inhomogenously-broadened and spatially-sequestered pore water is supported by observations of both its long T_2 ($\gg$ 1 ms) and short T_2* ($\approx$ 1 ms), as well as the poor inversion performance of narrow-band AFPs (Fig 4). Thus, the broad pore water NMR spectral line is interpreted as a superposition of chemically-shifted narrow lines that do not exchange significant magnetization with each other on the timescale of MRI measurements. This condition likely arises from expected magnetic susceptibility effects (27), a micro-anatomical pore size distribution (previously linked to the pore water T_2 distribution (15)), and the lack of rapid mixing across spatially-disparate pores. Importantly, at high fields this dictates that pore water is inhomogenously broadened to such an extent that some is likely to exhibit a T_2* similar to that of bound water. As such, the strongly multi-exponential nature of the cortical bone T_2 spectrum—with separable bound and pore water domains spanning several decades in T_2—is not preserved in the T_2* domain, and it will be challenging to quantitatively discriminate bound from pore water using spectroscopic imaging (30,31) or multiple gradient echo schemes adapted to uTE MRI. Additionally, straightforward chemical shift-based discrimination is impractical, given the similarly-broad and spectrally-overlapping bound and pore water lineshapes at high fields—lineshape differences between the two were not readily apparent in a previous study (13). An alternative scheme for pore/bound water discrimination is warranted for clinical and high field cortical bone MRI, and the concept of T_2-filtering bound from pore water with adiabatic pulses is explored herein.

Current Bone MRI Methods: Non-selective Imaging

Most cortical bone MRI to date has utilized broad-band excitation pulses and strategies for soft tissue suppression (6–8,32), but imaging results have not been well characterized with regards to bound vs. pore water contributions. BEuTE and CuTE were duplicated herein and did not exhibit significant bound/pore water discrimination. BEuTE's poor discrimination (Fig 5B) arises from a mixture of confounding factors, such as i) similar bound/pore water T_2*s that give rise to artifactual fitted signal fractions and ii) off-resonance effects from fat and other species that contribute non-monotonic characteristics to the FIDs and disrupt exponential fitting. Although short and long-T_2* fractions from high field imaging were attributed to bound and free water recently (31), the present findings suggest that such long-T_2* fractions do not capture all of the pore water contributions. We anticipate this will become even more problematic as bone imaging moves to higher fields (e.g. the 7T imaging shown in (36)), and further in vivo studies on this point are merited.

Since the CuTE signal includes both bound and pore water contributions, quantitation was performed with the net water T_1 (weighted average of bound and pore water), similar to the approaches taken by (3,6–8). Despite the observed ≈ 2-fold difference between bound and pore water T_1s, the CuTE signal agreed well with the net water content, showing a strong linear correlation and minimal bias (Fig 6D). Thus, this method is useful for net cortical bone water measurements, which supports the findings of other investigators (7).

AFP Pulses for Bound Water Selection

AFP-CPMG data (Fig. 4) showed that AFP pulses with bandwidths ≥ 2 kHz created a condition of strongly saturated bound water ($\alpha^{bw} \approx 0.1$) and well-inverted pore water ($\alpha^{pw} \approx -0.8$), which generates useful contrast between the two pools. For a variety of AFP pulse parameters and bandwidths ≥ 2 kHz, bone water behavior over a broad range of T_2s followed Bloch equation simulations (Fig. 2) but was not saturated/inverted as strongly as simulations predicted. This discrepancy may arise from unaccounted relaxation effects (e.g. $T_{1\rho}$) or from magnetization transfer (37) with a semisolid spin pool ($T_2 \approx 10$ μs) that would remain largely unaffected by the AFP pulses herein. However, evaluating such mechanisms is beyond the scope of this study. All AFP pulses with 1 kHz bandwidth still saturated bound water but failed to coherently invert the pore water, which is consistent with the model of homogeneously-broadened bound water and heterogeneously-broadened pore water. Thus, it appears that ≈ 2kHz is the minimum AFP bandwidth (at 4.7T) for effective manipulation of the pore water pool at high fields, and a 3.5 kHz bandwidth was used in the following.

DAFP for Pore Water-Selective Imaging

Incorporating a broadband DAFP pulse into steady-state imaging was found to strongly saturate bound water and result in a signal dominated by pore water (Fig 6B). The assumption that the observed DAFP signal arises entirely from pore water may contribute to overestimation of pore water content (Fig 6E), which is largely a consequence of signal contamination from incompletely saturated bound water and shorter-lived T_2s (≈ 50 μs) from collagen. However, there is still a strong correlation ($r^2 = 0.7$) between the DAFP signal and CPMG measures of pore water, even though sample-specific relaxation and AFP efficiency parameters were not included (i.e. population averages were used to scale the signal into proton concentration units). Thus, the DAFP signal is a useful measure of pore water. Unlike the AIR sequence, no prior information (e.g. R_1 estimates) is needed when planning the DAFP sequence timings. However, because of specific absorption rate constraints, the power deposition of DAFP pulses may lengthen the TR of the sequence relative to CuTE. For example, the DAFP sequence can be executed on our 3T clinical scanner with TR ≈ 80 ms, which can be further reduced by using higher-order hyperbolic secant (HSn) pulses (34).

AIR for Bound Water-Selective Imaging

The AIR approach has been successfully shown for general soft tissue suppression in cortical bone MRI (8,32), but its bound/pore water specificity has not been evaluated. Herein, it is shown that signal from an optimized AIR sequence (TR/TI = 300/90 ms) is dominated by bound water contributions and is largely insensitive to pore water (Fig 6C). Sources of bias in the signal quantitation include transverse relaxation during the *TE* period and magnetization transfer with a semisolids pool during the *TI* period. However, there was negligible bias, even without sample-specific relaxation or AFP efficiency correction, as seen by a strong correlation to reference-standard bound water measures ($r^2 = 0.91$, Fig 6F). Thus, the AIR signal provides a useful measure of bound water.

The high degree of AIR's bound water selectivity is advantageous, but it requires an estimate of pore water T_1 for optimal IR-nulling. Herein, a single empirically-determined 90

ms *TI* gave satisfactory pore water nulling across specimens, so a patient-specific estimate of pore water T_1 is not necessary for clinical bound water quantitation. However, since the pore water signal contains a distribution of T_1s, non-nulled pores with T_1s shorter and longer than the mean would be placed in anti-phase during bound water signal acquisition. To maintain this state and minimize pore water contamination, the imaging module in AIR should favor minimal echo and acquisition times.

Correlations to Mechanical Properties

Strong pairwise linear correlations ($r^2 \approx 0.3–0.7$) between various mechanical properties and the AIR and DAPF signals (Fig 7) provide a proof of concept that these strategies hold diagnostic relevance for predicting fracture risk. Importantly, donor-specific measures of bound/pore/net water T_1, T_2, and AFP pulse effects are not needed for mechanical property prediction (population averages were used herein) but may further strengthen correlations if available. The BEuTE fitted signal fractions, which were poor discriminators of bound/pore water, as well as the CuTE signal, which contains a mixture of both bound and pore water, were not found to have statistically significant correlations to any mechanical property, in agreement with our previous findings (18). In that study, with a three-fold-larger bone specimen population, both bound and pore water had similar mechanical correlation strengths. Herein, DAFP pore water showed considerably stronger mechanical correlations than AIR bound water, but the high correlation between the AIR-signal and equilibrium CPMG-derived bound water measures implies that stronger AIR/mechanical property correlations could emerge in a larger population. Additionally, there is likely to be an optimal imaging TE, since TE < 50 μs will introduce matrix-related signals ($T_2^* \approx 10$ μs, (11,13,17)) that confound pore water estimation, and TE > 50 μs enhances bound/pore water T_2^* weighting that may vary across bones in a manner not correlated with mechanical properties.

Finally, we note the possibility of combining any two of the CuTE/AIR/DAFP measurements to determine all three of S_0^{net}, S_0^{bw}, and S_0^{pw}. This follows the premise that $S_0^{net}=S_0^{bw}+S_0^{pw}$, where S_0^{net} is determined from CuTE and S_0^{bw} and S_0^{pw} are determined from AIR and DAFP, respectively. For example, the AIR sequence's maximum temporal signal-to-noise ratio efficiency, ($\propto S_{AIR}/\sqrt{TR}$), occurs at $TR \approx 500$ ms and $\theta \approx 90°$ for practical AFP and tissue characteristics ($\alpha^{bw} = 0.1$, $\alpha^{pw} = -0.85$, $R_1^{bw}=2.9\,\text{Hz}$, $R_1^{pw}=1.9\,\text{Hz}$). Such a long *TR* may be acceptable for 2D imaging, but 3D imaging may require impractically long scan times unless MP-RAGE (38) or similar acquisition schemes are employed to collect several lines of k-space during each *TR*. However, bound water information can be synthesized from two separate CuTE and DAFP scans in perhaps less time. Alternately, adding a small flip-angle imaging excitation to the AIR sequence immediately following the AFP pulse would provide a measure of pore water (bound water is relatively saturated at this point), and subsequent imaging after the *TI* period would give the bound water information demonstrated above, providing a complete measure of discriminated bone water in a single sequence. Thus, CuTE/DAFP/AIR sequences serve as building blocks for generating bound, pore, and/or net bone water maps.

Additionally, as an alternative to DAFP, we note that a spin echo measurement with a minimal (≈10 ms) echo time can, in principle, be used to selectively image the long-T_2 pore water (39) while allowing sufficient time for complete bound water T_2 decay, but the broad bandwidths needed to refocus the pore water spins will test the limits of clinical MRI (e.g. peak $|B_1|$ and specific absorption rate safeguards).

CONCLUSION

In summary, bound and pore water NMR signals in cortical bone follow homogeneously and in homogenously broadened transverse relaxation mechanisms, respectively. Bound and pore water-specific NMR spectra exhibit similar and overlapping lineshapes, so discriminating the two in commonly-used T_2* and chemical shift domains is challenging at high fields. We present alternate, T_2-filter-based strategies for isolating bound or pore water signals for uTE MRI. A pulse sequence (AIR) combining the T_2-selectivity of an AFP pulse and the T_1-selectivity of an inversion-recovery filter is demonstrated as a strategy for quantitative bound water imaging, and a double-AFP sequence (DAFP) is shown as a means for quantitative pore water imaging. Both methods achieve a high degree of bound/pore water selectivity while utilizing clinically-relevant RF pulse parameters. The resulting signals have strong correlation to important bone mechanical properties, which was not found to be the case for current bone imaging methods (BEuTE/CuTE). Since patient-specific measures of T_1 and T_2 (i.e. AFP pulse effects) are not needed, it should be practical to obtain *in vivo* bound and pore water maps of cortical bone with the proposed methods, which may be used to assess bone fracture risk in conjunction with structural parameters.

Acknowledgments

We are grateful to our grant sponsors: NIH #EB001744, Vanderbilt Discovery Grant, Air Force Office of Scientific Research #32CFR168a (NDSEG).

References

1. Robson MD, Gatehouse PD, Bydder M, Bydder GM. Magnetic resonance: An introduction to ultrashort TE (UTE) imaging. J Comput Assist Tomogr. 2003; 27(6):825–846. [PubMed: 14600447]
2. Idiyatullin D, Corum C, Park J, Garwood M. Fast and quiet MRI using a swept radiofrequency. J Magn Reson. 2006; 181(2):342–349. [PubMed: 16782371]
3. Wu Y, Ackerman J, Chesler D, Graham L, Wang Y, Glimcher M. Density of organic matrix of native mineralized bone measured by water- and fat-suppressed proton projection MRI. Magn Reson Med. 2003; 50(1):59–68. [PubMed: 12815679]
4. Balcom B, MacGregor R, Beyea S, Green D, Armstrong R, Bremner T. Single-point ramped imaging with T-1 enhancement (SPRITE). J Magn Reson A. 1996; 123(1):131–134. [PubMed: 8980075]
5. Du J, Takahashi AM, Chung CB. Ultrashort TE Spectroscopic Imaging (UTESI): Application to the Imaging of Short T2 Relaxation Tissues in the Musculoskeletal System. J Magn Reson Imaging. 2009; 29(2):412–421. [PubMed: 19161197]
6. Techawiboonwong A, Song H, Leonard M, Wehrli F. Cortical bone water: In vivo quantification with ultrashort echo-time MR imaging. Radiology. 2008; 248(3):824–833. [PubMed: 18632530]
7. Rad HS, Lam SCB, Magland JF, Ong H, Li C, Song HK, Love J, Wehrli FW. Quantifying cortical bone water in vivo by three-dimensional ultra-short echo-time MRI. NMR Biomed. 2011; 24(7): 855–864. [PubMed: 21274960]
8. Du J, Carl M, Bydder M, Takahashi A, Chung CB, Bydder GM. Qualitative and quantitative ultrashort echo time (UTE) imaging of cortical bone. J Magn Reson. 2010; 207(2):304–311. [PubMed: 20980179]
9. Springer F, Martirosian P, Machann J, Schwenzer N, Claussen C, Schick F. Magnetization Transfer Contrast Imaging in Bovine and Human Cortical Bone Applying an Ultrashort Echo Time Sequence at 3 Tesla. Magn Reson Med. 2009; 61(5):1040–1048. [PubMed: 19267348]
10. Ni Q, Nicolella D. The characterization of human cortical bone microdamage by nuclear magnetic resonance. Meas Sci Technol. 2005; 16(3):659–668.

11. Nyman J, Ni Q, Nicolella D, Wang X. Measurements of mobile and bound water by nuclear magnetic resonance correlate with mechanical properties of bone. Bone. 2008; 42(1):193–199. [PubMed: 17964874]
12. Fernandez-Seara M, Wehrli S, Takahashi M, Wehrli F. Water content measured by proton-deuteron exchange NMR predicts bone mineral density and mechanical properties. J Bone Miner Res. 2004; 19(2):289–296. [PubMed: 14969399]
13. Horch R, Nyman J, Gochberg D, Dortch R, Does M. Characterization of 1H NMR signal in human cortical bone for magnetic resonance imaging. Magn Reson Med. 2010; 64(3):680–687. [PubMed: 20806375]
14. Fantazzini P, Brown R, Borgia G. Bone tissue and porous media: common features and differences studied by NMR relaxation. Magn Reson Imaging. 2003; 21(3–4):227–234. [PubMed: 12850712]
15. Ni Q, King J, Wang X. The characterization of human compact bone structure changes by low-field nuclear magnetic resonance. Meas Sci Technol. 2004; 15(1):58–66.
16. Wang X, Ni Q. Determination of cortical bone porosity and pore size distribution using a low field pulsed NMR approach. J Orthop Res. 2003; 21(2):312–319. [PubMed: 12568964]
17. Ni Q, Nyman J, Wang X, De Los Santos A, Nicolella D. Assessment of water distribution changes in human cortical bone by nuclear magnetic resonance. Meas Sci Technol. 2007; 18(3):715–723.
18. Horch RA, Gochberg DF, Nyman JS, Does MD. Non-invasive Predictors of Human Cortical Bone Mechanical Properties: T-2-Discriminated H-1 NMR Compared with High Resolution X-ray. PLoS ONE. 2011; 6(1):e16359. [PubMed: 21283693]
19. Carl M, Bydder M, Du J, Takahashi A, Han E. Optimization of RF excitation to maximize signal and T2 contrast of tissues with rapid transverse relaxation. Magn Reson Med. 2010; 64(2):481–490. [PubMed: 20665792]
20. Josan S, Pauly JM, Daniel BL, Pauly KB. Double Half RF Pulses for Reduced Sensitivity to Eddy Currents in UTE Imaging. Magn Reson Med. 2009; 61(5):1083–1089. [PubMed: 19235919]
21. Larson PEZ, Gurney PT, Nayak K, Gold GE, Pauly JM, Nishimura DG. Designing long-T-2 suppression pulses for ultrashort echo time imaging. Magn Reson Med. 2006; 56(1):94–103. [PubMed: 16724304]
22. Larson PEZ, Conolly SM, Pauly JM, Nishimura DG. Using adiabatic inversion pulses for long-T-2 suppression in ultrashort echo time (UTE) imaging. Magn Reson Med. 2007; 58(5):952–961. [PubMed: 17969119]
23. Sussman M, Pauly J, Wright G. Design of practical T-2-selective RF excitation (TELEX) pulses. Magn Reson Med. 1998; 40(6):890–899. [PubMed: 9840834]
24. Silver M, Joseph R, Hoult D. Highly selective $\pi/2$ and π pulse generation. J Magn Reson. 1984; 59(2):347–351.
25. Norris D, Ludemann H, Leibfritz D. An Analysis of the Effects of Short T2 Values on the Hyperbolic-Secant Pulse. J Magn Reson. 1991; 92(1):94–101.
26. Cowin S. Bone poroelasticity. J Biomech. 1999; 32(3):217–238. [PubMed: 10093022]
27. Hopkins J, Wehrli F. Magnetic susceptibility measurement of insoluble solids by NMR: Magnetic susceptibility of bone. Magn Reson Med. 1997; 37(4):494–500. [PubMed: 9094070]
28. Wehrli F, Fernandez-Seara M. Nuclear magnetic resonance studies of bone water. Ann Biomed Eng. 2005; 33(1):79–86. [PubMed: 15709708]
29. Bull T. Relaxation in the rotating frame in liquids. Prog Nucl Magn Reson Spectrosc. 1992; 24:377–410.
30. Du J, Hamilton G, Takahashi A, Bydder M, Chung C. Ultrashort echo time spectroscopic imaging (UTESI) of cortical bone. Magn Reson Med. 2007; 58(5):1001–1009. [PubMed: 17969110]
31. Diaz E, Chung C, Bae W, Statum S. Ultrashort echo time spectroscopic imaging (UTESI): an efficient method for quantifying bound and free water. NMR Biomed. 2011 (available online in early view).
32. Du J, Takahashi AM, Bae WC, Chung CB, Bydder GM. Dual Inversion Recovery, Ultrashort Echo Time (DIR UTE) Imaging: Creating High Contrast for Short-T-2 Species. Magn Reson Med. 2010; 63(2):447–455. [PubMed: 20099332]

33. Horch RA, Wilkens K, Gochberg DF, Does MD. RF coil considerations for short-T2 MRI. Magn Reson Med. 2010; 64(6):1652–1657. [PubMed: 20665825]

34. Tannus A, Garwood M. Improved performance of frequency-swept pulses using offset-independent adiabaticity. J Magn Reson A. 1996; 120(1):133–137.

35. Fernandez-Seara M, Wehrli S, Wehrli F. Diffusion of exchangeable water in cortical bone studied by nuclear magnetic resonance. Biophys J. 2002; 82(1):522–529. [PubMed: 11751339]

36. Krug R, Larson PEZ, Wang C, Burghardt AJ, Kelley DAC, Link TM, Zhang X, Vigneron DB, Majumdar S. Ultrashort echo time MRI of cortical bone at 7 tesla field strength: A feasibility study. J Magn Reson Imaging. 2011; 34(3):691–695. [PubMed: 21769960]

37. Springer F, Martirosian P, Machann J, Schwenzer NF, Claussen CD, Schick F. Magnetization Transfer Contrast Imaging in Bovine and Human Cortical Bone Applying an Ultrashort Echo Time Sequence at 3 Tesla. Magn Reson Med. 2009; 61:1040–1048. [PubMed: 19267348]

38. Haase A. Snapshot FLASH MRI. Applications to T1, T2, and Chemical Shift Imaging. Magn Reson Med. 1990; 13(1):77–89. [PubMed: 2319937]

39. Du, J. ISMRM Workshop on MSK. 2009. Assessment of cortical bone structure with FSE, 2D and 3D UTE sequences.

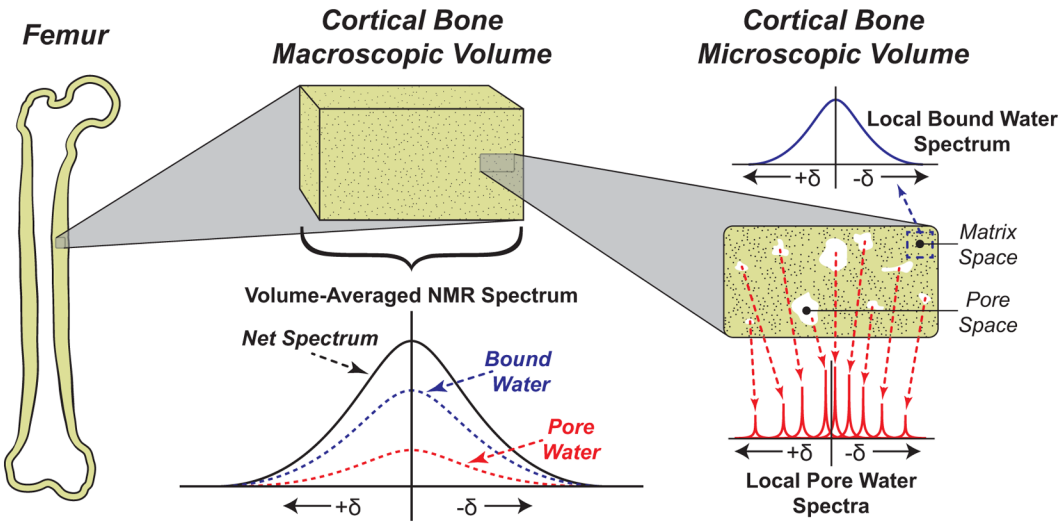

FIGURE 1. A model of the water ^{1}H NMR lineshapes in human cortical bone

Across a macroscopic volume of cortical bone akin to an MRI voxel (middle), numerous bound and pore water components are combined into a broad net NMR spectrum with similarly broadened bound and pore water contributions. On the local microscale (right), bound water in the bone matrix space gives rise to a homogeneously broadened NMR spectrum. Conversely, the relatively mobile water within each pore space gives rise to a narrower NMR spectrum of varied chemical shift (dictated by pore geometry and pore-matrix susceptibility variation). The sum of these microscale contributions gives rise to a heterogeneously broadened pore water lineshape across macroscopic bone volumes (middle).

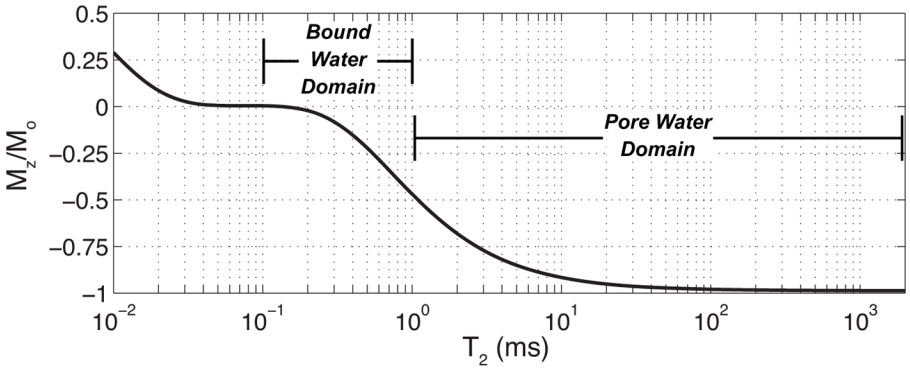

FIGURE 2. Simulated effects of a sech AFP pulse on cortical bone water longitudinal magnetization

Bloch equation simulation of a 5ms/5kHz AFP shows a significant T_2 dependence of the AFP inversion efficiency (above). Such an AFP pulse is expected to largely saturate and invert the bound and pore water magnetizations, respectively, given their considerably different T_2 domains noted above.

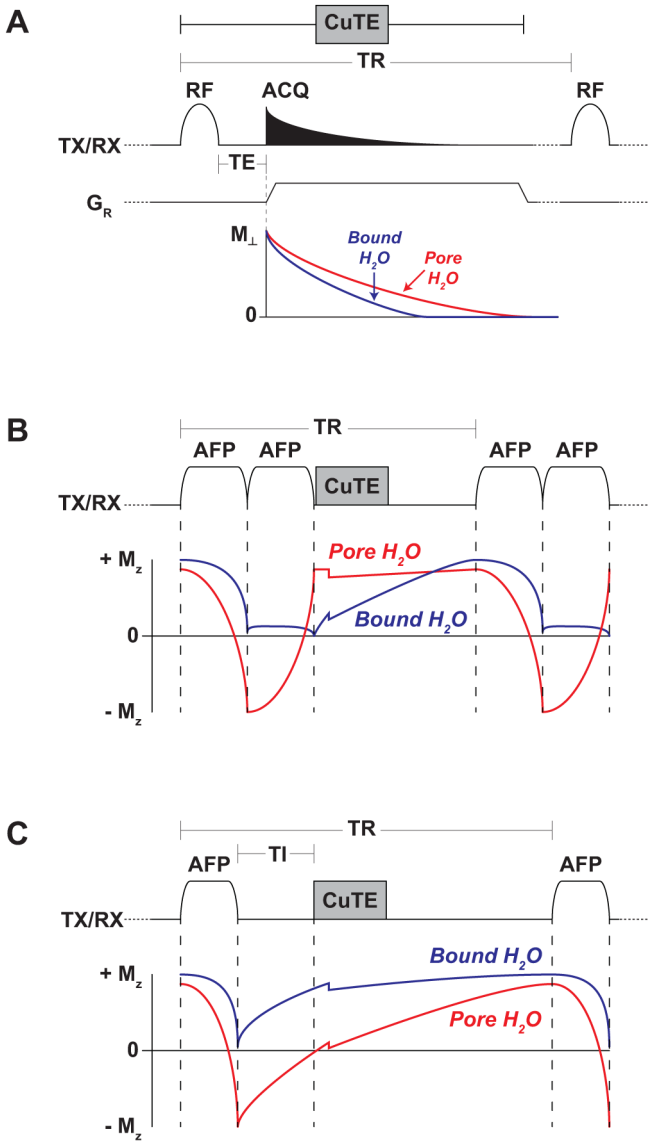

FIGURE 3. The proposed ultra-short echo time-based approaches for MRI of cortical bone net, pore, and bound water content

The CuTE sequence in A is sensitive to both bound and pore water, but their similar T_2* present difficulties in quantitatively distinguishing bound from pore water if spectroscopic acquisition schemes are employed for BEuTE (see subplot). Incorporating a double-AFP T_2 filter (DAFP) into the uTE sequence (B) drives the steady state bound water longitudinal magnetization to saturation at readout, thus creating a signal dominated by pore water. Conversely, the adiabatic inversion recovery (AIR) scheme in C drives pore water to saturation, creating a predominantly bound water signal. (TR=repetition time, TI=inversion time, G_R= readout gradient, RF=slice or volume excitation).

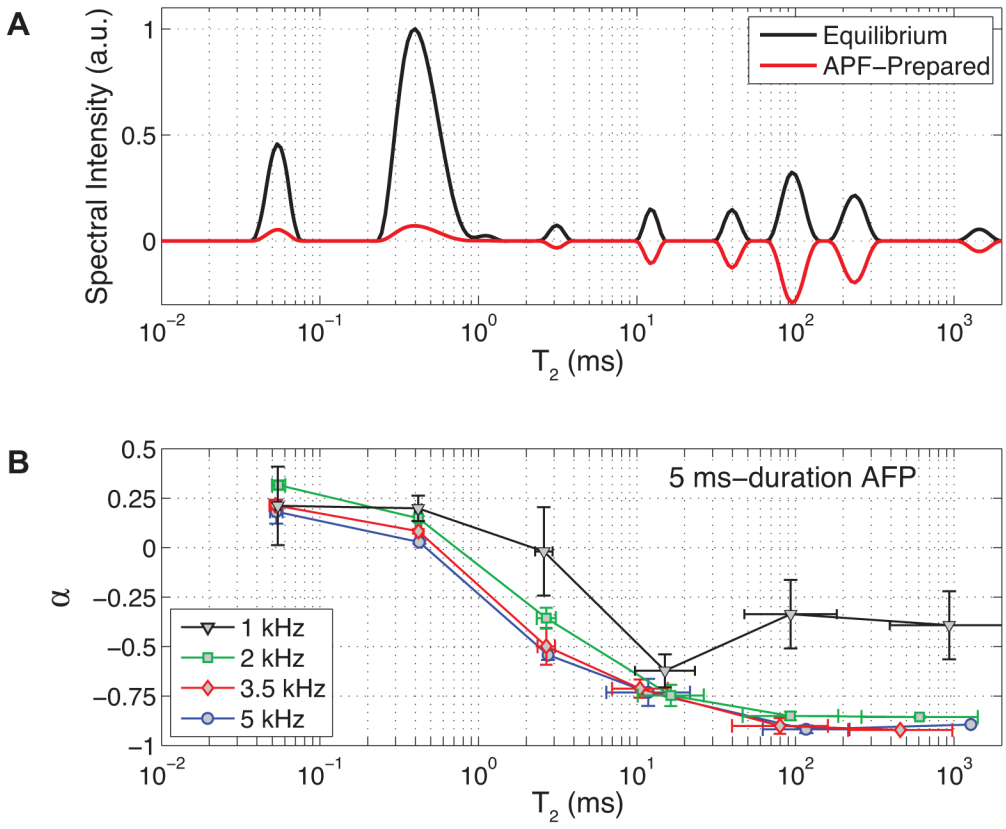

FIGURE 4. Observed effects of a sech AFP pulse on cortical bone water longitudinal magnetization

T_2 spectra (A) from a representative bone specimen at equilibrium and following an AFP pulse (5ms/5kHz) show a largely saturated bound water component ($T_2 \approx 0.4$ ms) and inverted pore water ($T_2 > 1$ ms), as represented by the negative spectral amplitudes (see Methods for details). The ratio of AFP-prepared to equilibrium T_2 spectral peak areas gives the APF efficiency parameter α, shown in B for a variety of AFP bandwidths (error bars represent ±1 SD across specimens).

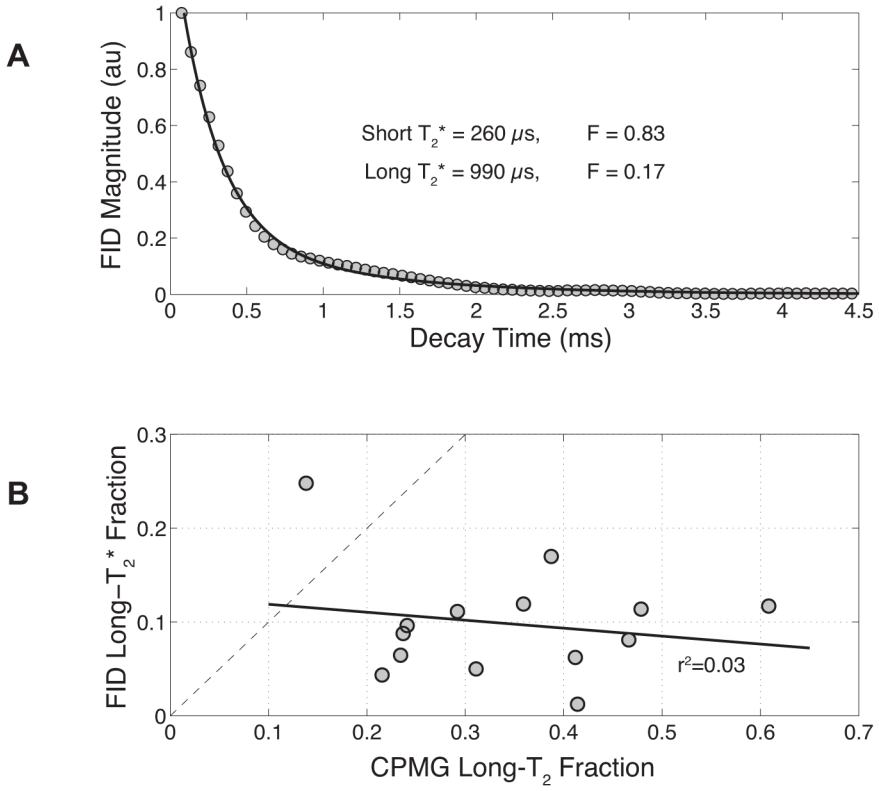

FIGURE 5. Bi-exponential fitting for bound/pore water separation in the T_2* domain

A representative cortical bone equilibrium FID and bi-exponential fit is shown with resulting T_2 and signal fraction values at inset (A). Across the specimens (B), the long-T_2* signal fraction obtained from FID bi-exponential fitting was poorly correlated to the long-T_2 (1ms < T_2 < 1s) signal fraction obtained from CPMG multi-exponential fitting, the latter of which is known to arise predominantly from pore water. Thus, FID data were poor indicators of pore water content.

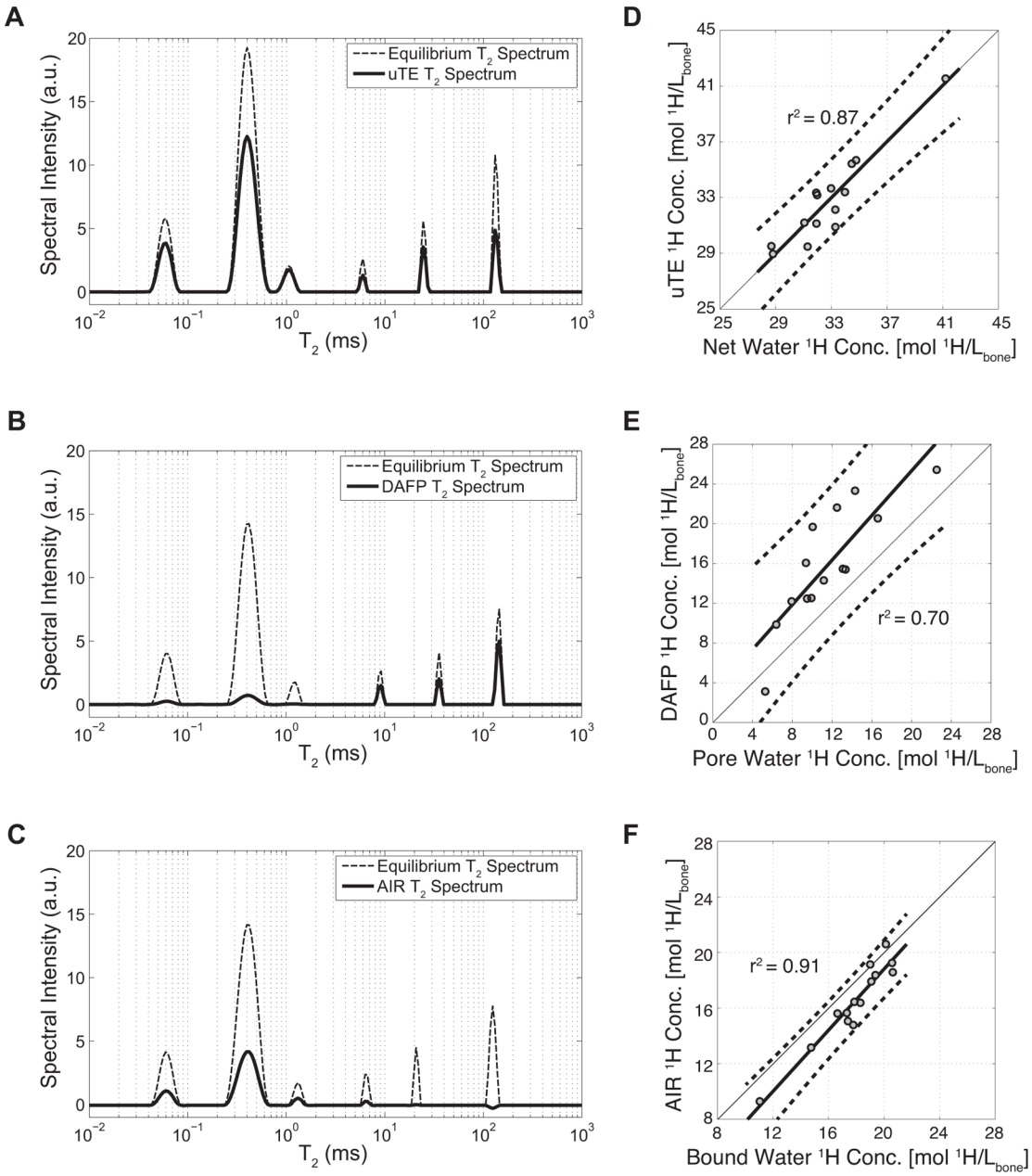

FIGURE 6. Signal contents and correlations to reference standard measures for the uTE, DAFP, and AIR methods

T_2 spectra from CPMGs collected at steady state show that the net uTE signal contains a mixture of both bound and pore water contributions (A), while the DAFP signal is dominated by pore water (B) and the AIR signal by bound water (C). For each method (D–F), estimates of M_o from the steady state FID signal—quantified in absolute units of proton concentration—correlated satisfactorily to reference-standard measures of net, pore, or bound water as determined by equilibrium T_2 spectroscopy.

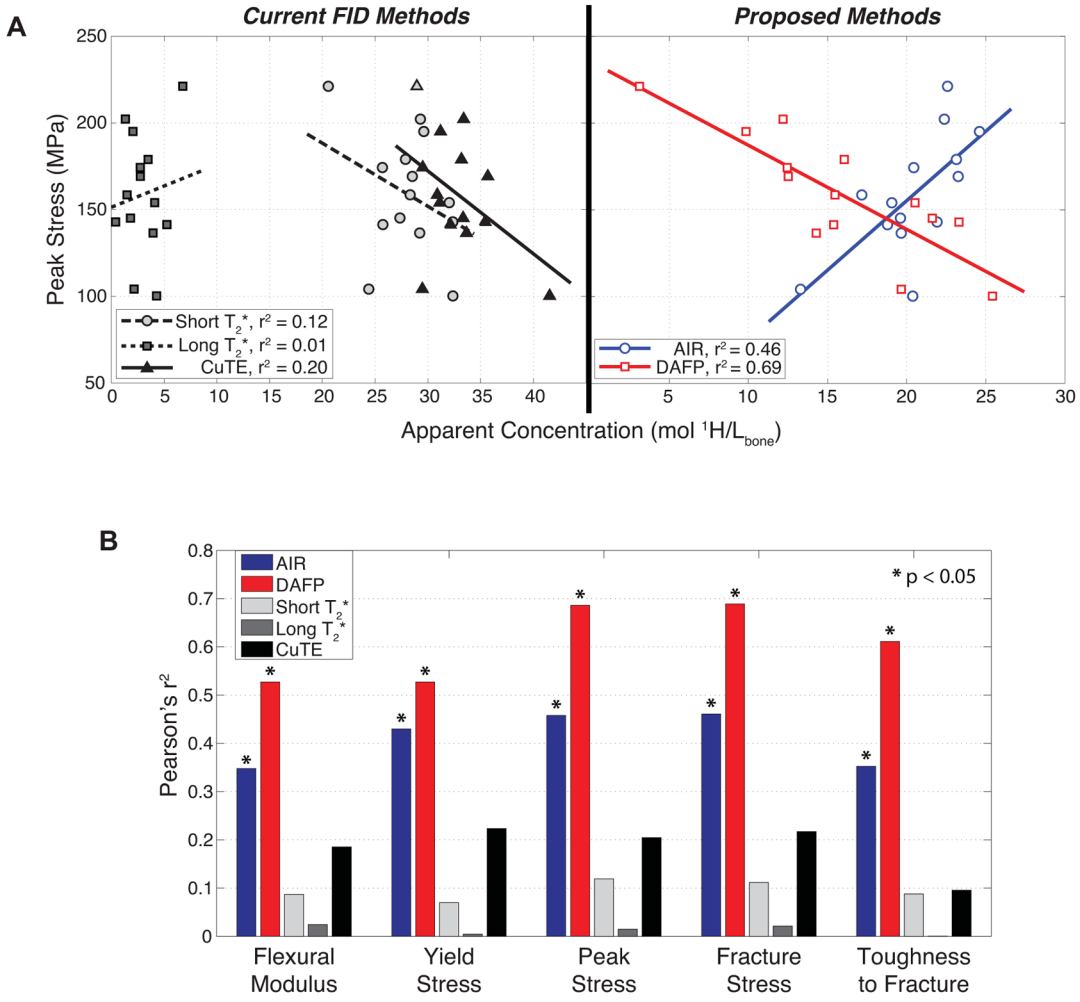

FIGURE 7. Mechanical property correlations to steady state signals across specimens

Linear correlations to peak stress are shown for proton concentrations derived from BEuTE (short/long-T_2*) and CuTE methods (A, left) as well as for concentrations derived from the proposed AIR/DAFP methods (A, right). Pearson's r^2s for correlations between the different methods' water concentrations and various mechanical properties are summarized in B. While AIR and DAFP were good correlates to mechanical properties, none of the FID methods exhibit statistically significant correlations ($p < 0.05$) for any of the mechanical properties surveyed.